A review of *β*-Ga$_2$O$_3$ single crystal defects, their effects on device performance and their formation mechanism

Bo Fu, Zhitai Jia†, Wenxiang Mu, Yanru Yin, Jian Zhang, and Xutang Tao†

State Key Laboratory of Crystal Materials & Key Laboratory of Functional Crystal Materials and Device, Shandong University, Jinan 250100, China

Abstract: As a wide-bandgap semiconductor (WBG), *β*-Ga$_2$O$_3$ is expected to be applied to power electronics and solar blind UV photodetectors. In this review, defects in *β*-Ga$_2$O$_3$ single crystals were summarized, including dislocations, voids, twin, and small defects. Their effects on device performance were discussed. Dislocations and their surrounding regions can act as paths for the leakage current of SBD in single crystals. However, not all voids lead to leakage current. There's no strong evidence yet to show small defects affect the electrical properties. Doping impurity was definitely irrelated to the leakage current. Finally, the formation mechanism of the defects was analyzed. Most small defects were induced by mechanical damages. The screw dislocation originated from a subgrain boundary. The edge dislocation lying on a plane slightly tilted towards the (102) plane, the (101) being the possible slip plane. The voids defects like hollow nanopipes, PNPs, NSGs and line-shaped grooves may be caused by the condensation of excess oxygen vacancies, penetration of tiny bubbles or local meltback. The nucleation of twin lamellae occurred at the initial stage of "shoulder part" during the crystal growth. These results are helpful in controlling the occurrence of crystal defects and improving the device performance.

Key words: *β*-Ga$_2$O$_3$; crystal defects; device performance; formation mechanism

1. Introduction

Recently, *β*-Ga$_2$O$_3$ has attracted great attention as an ultra wide band-gap oxide semiconductor for future power and photodetector devices. In order to achieve high-performance and high-reliability of semiconductor devices, it is critical to control crystal defects because those defects could have negative and damaging effects on the device performance. In some cases, those crystal defects can even bring about leakage current and lower breakdown voltage, such as micropipes observed in SiC. Thus, it is essential to characterize defects in the crystal and understand their formation mechanism.

The crystal structure of *β*-Ga$_2$O$_3$ is shown in Fig. 1. *β*-Ga$_2$O$_3$ is the most thermodynamically stable one in terms of the six different phases of the *α*, *β*, *γ*, *δ*, *ε*, and *φ* phases[1]. *β*-Ga$_2$O$_3$ belongs to monoclinic system with lattice constants of *a* = 1.223 nm, *b* = 0.304 nm, and *c* = 0.580 nm, and the angle between the *a*- and *c*-axes is *β* = 103.7°[2]. There exist two inequivalent Ga sites and three inequivalent O sites, denoted by Ga(I), Ga(II), O(I), O(II), and O(III) atoms, respectively. Ga(I) atoms form slightly distorted tetrahedral bonds with 4 O ions, and Ga(II) atoms form a highly distorted cubic close packing arrangement with 6 neighboring O ions. O(I) and O(II) are 3-fold-coordinated, whereas O(III) is 4-fold-coordinated at the corner of three octahedra and one tetrahedron[3–5].

The melting point of Ga$_2$O$_3$ is approximately 1800 °C[36]. In order to obtain large size crystal combined with high structural quality, melt growth methods are the most suitable, especially when they are used for industrial production. A few melt

growth techniques have been used to grow bulk *β*-Ga$_2$O$_3$ single crystals successfully, such as Verneuil[6–8], Optical Floating Zone (OFZ)[9–11], Vertical Bridgman (VB)/Vertical Gradient Freeze (VGF)[12, 13], Edge-Defined Film-Fed Growth (EFG)[14–17] and the Czochralski methods[18–23]. The flux[24, 25] and gas phase[26, 27] methods have also been applied to the growth of *β*-Ga$_2$O$_3$. However, the obtained crystal size is too small for applications, so these methods are not considered here. Similarly, the Verneuil method is also not introduced in this review considering the imperfect *β*-Ga$_2$O$_3$ crystal quality and inadequate crystal size (only 10 mm in diameter).
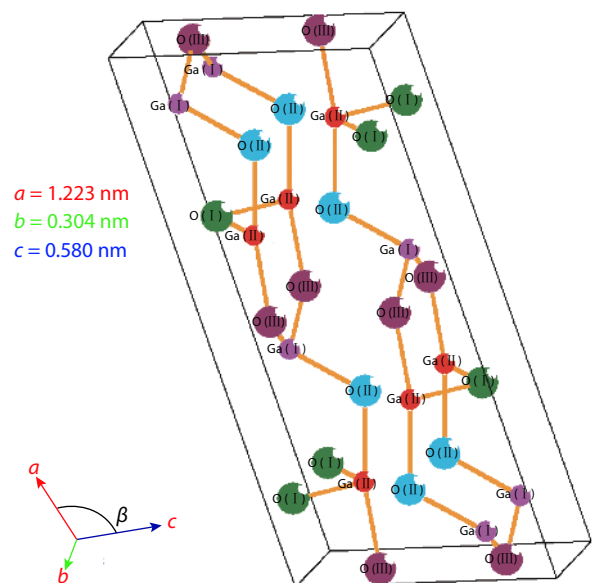

a = 1.223 nm
b = 0.304 nm
c = 0.580 nm

Fig. 1. (Color online) Monoclinic unit cell of *β*-Ga$_2$O$_3$ and relative lattice parameters.

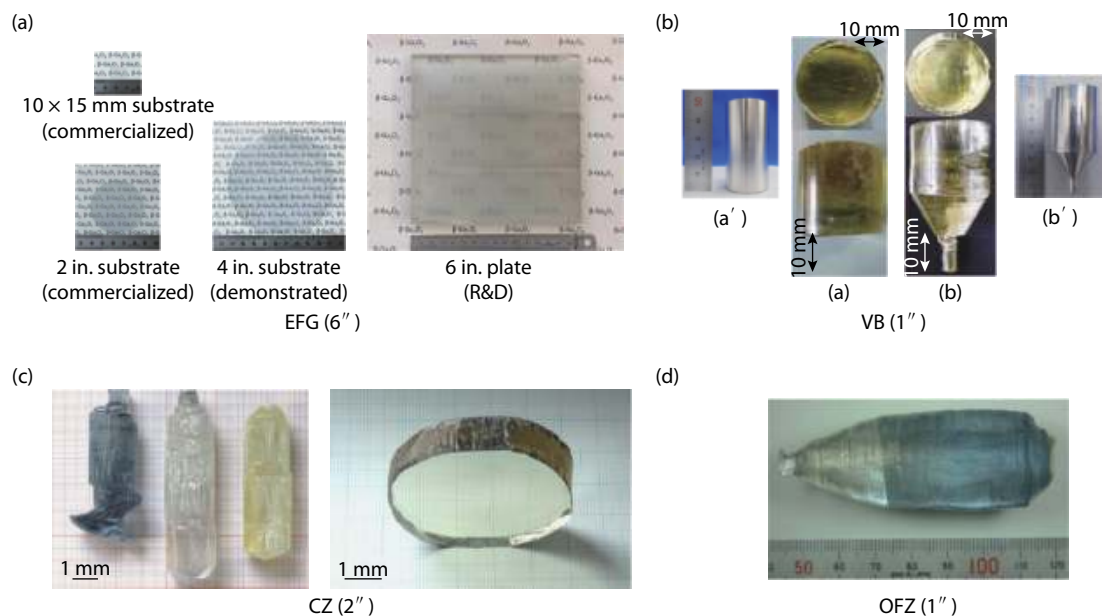Correspondence to: Z T Jia, z.jia@sdu.edu.cn; X T Tao, txt@sdu.edu.cn

Fig. 2. (Color online) Bulk β-Ga$_2$O$_3$ crystals obtained by the following melt methods: (a) EFG, (b) VB, (c) Czochralski, and (d) OFZ. Copyright 2017 ECS Journal of Solid State Science and Technology[28]. Copyright 2016 J Cryst Growth[13]. Copyright 2014 J Cryst Growth[47]. Copyright 2004 J Cryst Growth[11].
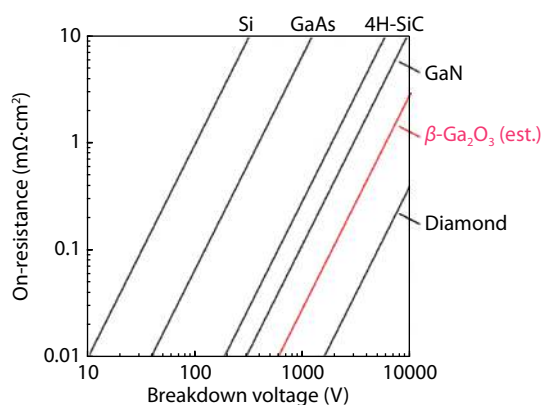

Fig. 3. (Color online) Theoretical limits of on-resistance versus breakdown voltage in unipolar power devices for β-Ga$_2$O$_3$ and other major semiconductors. Copyright 2014 Physical Status Solidi[29].

Fig. 4. Cross-sectional TEM image of a dislocation viewed from $[\bar{1}0\bar{2}]$. Copyright 2015 Jpn J Appl Phys[38].

Fig. 2 showed the examples of bulk β-Ga$_2$O$_3$ single crystals obtained by melt growth methods: (a) EFG, (b) VB, (c) Czochralski and (d) OFZ. The EFG method employs a die or a shaper that is placed in a metal crucible. The melt is transported from the crucible to a shaped top surface of the die by a narrow slit or channel due to capillary forces. The growth direction is always along the [010] crystallographic direction, which is paralleled to both cleavage planes (100) and (001). Presently, the EFG method is able to fabricate substrate of 2″ (commercialized), 4″ (demonstrated), and possible 6″ (under research & development) as shown in Fig. 2(a). The VB method utilizing a Pt-Rh (70%–30%) alloy crucible to grow β-Ga$_2$O$_3$ single crystal is in development, which is favorable for high oxygen concentration. The crystal of 25 mm in diameter is grown in air without a crystal seed as shown in Fig. 2(b). As for the crystal growth by Czochralski method, crystal spiral growth turns out to be the main challenge. However, the novel approach with a CO$_2$-containing growth atmosphere providing oxygen partial pressures, allows to obtain 2″ in diameter crystals as
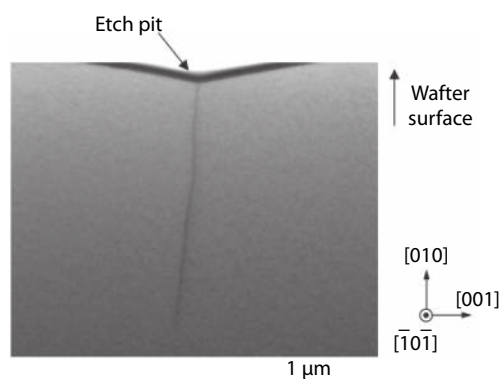
shown in Fig. 2(c). The OFZ method is a crucible-free technique. The main advantage of this method is the possibility of using highly oxidizing atmosphere to suppress the volatilization of β-Ga$_2$O$_3$. Crystals with 1 in. diameter have been reported as shown in Fig. 2(d).

β-Ga$_2$O$_3$ has attracted much interest as a substrate to grow GaN heteroepitaxy for efficient high-brightness vertically-structured LEDs due to its good conductivity and nice transparency[30, 31]. In addition, its most potential application fields are solar-blind UV photodetectors and high power devices. Because of its ultra wide band gap, 4.9 eV, β-Ga$_2$O$_3$ is highly transparent from the visible to the deep UV region and has an extremely high theoretical breakdown electric field (E_{br}) of 8 MV/cm[32]. The potential advantage of β-Ga$_2$O$_3$ is well described by the Baliga's figure of merit (BFOM) which indicates its basic suitability as a semiconductor material for high power applications[2]. β-Ga$_2$O$_3$ has a BFOM about 3000, 10 and 4 times higher than that of Si, SiC and GaN, respectively. This result is graphically depicted in Fig. 3, which showed the theoretical limits of the on-resistance as a function of breakdown voltage for the most studied semiconductors. Due to a much
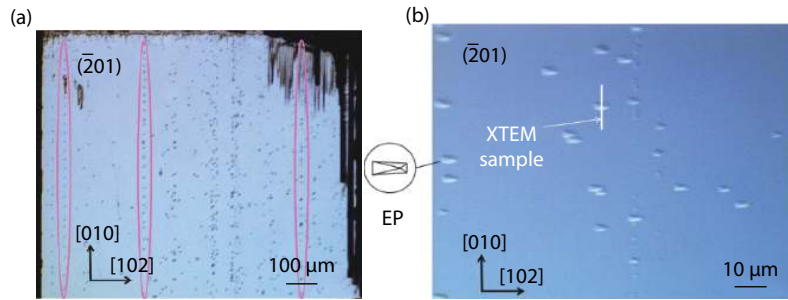
Fig. 5. (Color online) (a) Optical micrograph of surface of ($\bar{2}$01) plane after etching. (b) Enlarged image of the etch pits. An XTEM sample is indicated by a white line. Copyright 2016 Jpn J Appl Phys[39].
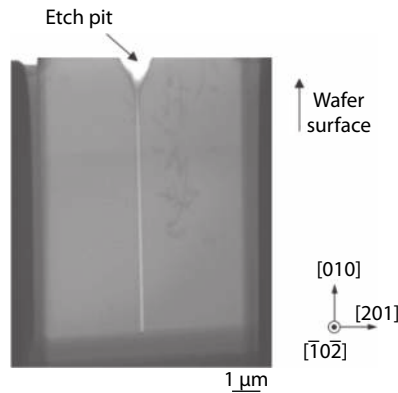

Fig. 6. Cross-sectional TEM image of a hollow nanopipes defect viewed from [$\bar{1}$0$\bar{2}$]. Copyright 2015 Jpn J Appl Phys[38].

higher BFOM, β-Ga$_2$O$_3$ is predicted to outperform SiC and GaN, meanwhile exceeds the physical limits of Si for power switching applications[33]. Despite of the relatively low electron mobility limited to 200 cm^{2}V^{-1}s^{-1} by calculation[34], the drastic reduction of the distance between gate and drain will allow the fabrication of high efficient semiconductor switches. Furthermore, compared with SiC and GaN[35], β-Ga$_2$O$_3$ has a relatively low thermal conductivity. Therefore, the development of thermally stable metal contacts and passivation layers would make up for this disadvantage and allow β-Ga$_2$O$_3$-based power electronics to operate under comparatively high temperature.

In this review, we summarize all kinds of defects observed in β-Ga$_2$O$_3$ single crystal recently. Subsequently, the effects of defects on device performance and their formation mechanism are summarized and analyzed in detail, which will provide a basis reference for device performance improvement in the future.

2. Four types of defects in β-Ga$_2$O$_3$ single crystal

2.1. Dislocations

The dislocations can be divided into two types, screw dislocation and edge dislocation. Nakai et al. found out the screw dislocations on the (010) plane[38], as shown in Fig. 4. The dislocation under etch pit was almost paralleled to [010]. The etch pits of dislocation were approximately 2μm in length and 10^6–10^7 cm^{-2} in density. Most of etch pits align in rows along [100] and [102]. According to the $\boldsymbol{g} \cdot \boldsymbol{b}$ invisibility criterion[42], the Burgers vector of dislocations were determined to parallel to [010]. Therefore, the dislocation was defined as screw dislocation because the Burgers vector and dislocation were both par-

alleled to [010] direction.

Ueda et al. reported the edge dislocation on the ($\bar{2}$01) plane[39], as shown in Fig. 5. The etch pits of edge dislocation mostly lied in a row along the [010] direction as shown in Fig. 5(a). The estimated etch pit density was 10^4 cm^{-2}. The distance between the etch pits varied in the range 20–100 μm. Apart from these pits, isolated etch pits were also observed as shown in Fig. 5(b). The result suggested that the etch pit was four-faceted with a core inside, the surface being rectangular in shape. Its long axis was in the [102] direction. The core of the etch pit was slightly off-centered. According to $\boldsymbol{g} \cdot \boldsymbol{b}$ invisibility criterion similar to the determination of screw dislocation, it can be clearly indicated that the defect under the etch pit was an edge dislocation because the Burgers vector was perpendicular to dislocation direction.

2.2. Voids

The voids defect has some volume, and thus can be observed on different crystal planes, including hollow nanopipes[38], platelike nanopipes (PNPs)[39], nanometer-sized grooves (NSGs)[40] and line-shaped grooves[44]. Nanopipes were hollow characterized by electron diffraction patterns and EDS. Its size was 0.1 μm in diameter and at least 15 μm in length elongated along [010] because the bottom end of the defect was not located in the TEM sample, as shown in Fig. 6. No strain field was found around them. The etch pits distribution of hollow nanopipes showed no significant orientation, with a density of 10^2 cm^{-2}.

A very narrow groove[39] goes deep into the crystal, thus, the defect is called platelike nanopie on the (010) plane as shown in Fig. 7(a) which is different from hollow nanopipe in Fig. 6. The etch pits of PNPs was along the (010) plane and parallelogram-shaped. The PNPs was hollow, too. In addition, Nanometer-sized grooves also were found on the (010) plane[40]. The NSGs length ranged from 50–1200 nm in the [001] direction, and the width of most grooves was approximately 40 nm in the [100] direction as shown in Fig. 7(b). The main sidewalls in the grooves were (100) and (001) because they were both thermodynamically stable planes. These NSGs tended to be generated along the [001] direction. All NSGs should terminate within crystal because the grooves disappeared gradually with the etching time. The depth was estimated to be roughly 30 nm. The NSGs were different from micropipes found in SiC crystal[37, 41] that penetrate the whole crystal.

Numerous line-shaped grooves[44] extended along the [010] direction and broadened along the [100] direction on the (001) plane as shown in Fig. 8. Such line-shaped defects existed not only on the etched surface but also inside the crystal,
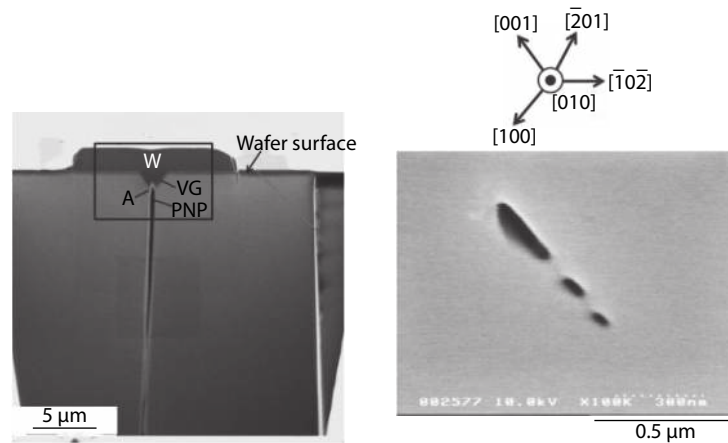
Fig. 7. (a) A cross-sectional FIB-SIM image of an PNPs defects. Copyright 2016 Jpn J Appl Phys[39]. (b) SEM image of three NSGs in an array along the [001] direction. Copyright 2016 Jpn J Appl Phys[40].
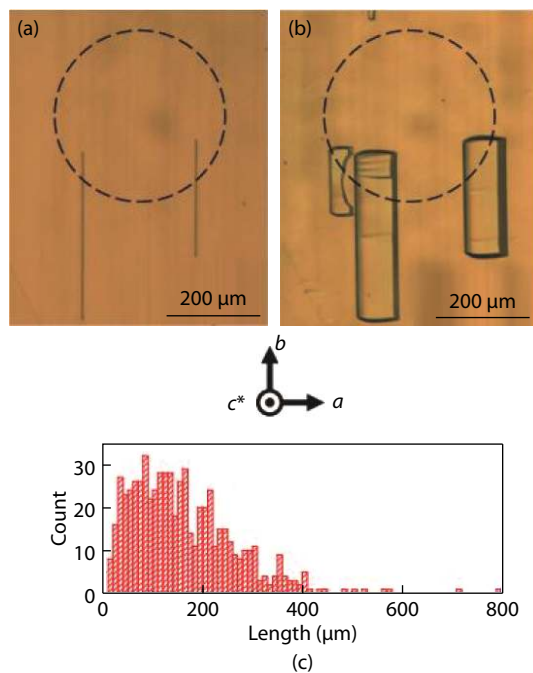

Fig. 8. (Color online) DICM images showing line-shaped voids exposed on the surface etching for (a) 5 min and (b) 25 min. (c) Length histogram of the 625 line-shaped voids observed on the 5-min etched surface. Copyright 2017 Jpn J Appl Phys[44].

and can be regarded as voids because these defects had some volume. The etched line-shaped grooves density near the surface was approximately 3×10^2 cm^{-2}. The length of the grooves along [010] varied from 10–400 μm. In addition, a line-shaped etch pattern was also found on the $(\bar{2}01)$ plane by Kasu *et al.*[45]. The defect was the same as those observed by Kuramata *et al.*[46].

2.3. Twin

A large number of defects were reported on (010), (001), and $(\bar{2}01)$ crystal planes. In contrast, the defects reported on (100) is very rare. Galazka *et al.* even considered the (100) plane as almost dislocation-free plane because the dislocations were all parallel to the (100) cleavage plane and did not lead to etch pits on (100) surface at all[47]. However, an important defect, twin, was observed on the (100) plane[39]. The

shapes of the etch pits corresponding to the defects of PNPs on both sides of the dotted line had mirror symmetry. The plane corresponding to the dotted line was a (100) twin boundary also shown in Fig. 9(a). A schematic diagram of the atomic structure of the twin lamellae is shown in Fig. 9(b).

2.4. Small defects

Apart from the mentioned defects above, small defects were also found. However, the small defects exist in the shape of different types of etch pits, including arrow-shaped etch pit[44, 45] and gourd-shaped etch pit[45]. The arrow's head faced toward the [102] direction. Some of the etch pits tended to form an array toward the [010] direction. Fig. 10 showed an AFM image of the arrow-shaped etch pit. The average density was 7×10^4 cm^{-2}. The depth of the etch pit was approximately 600 nm. The origin of the arrow-shaped etch pit was predicted to be from a dislocation.

Fig. 11 showed the AFM image of a gourd-shaped etch pit. The point head faced toward the [102] direction. The average density was 9×10^4 cm^{-2}. The depth of the gourd-shaped etch pit was 25 nm, which was much less than that of the arrow-shaped etch pit (600 nm). Thus, the gourd-shaped etch pit tended to be shallower than the arrow-shaped etch pit. Some gourd-shaped etch pits also tended to form an array along the [010] direction. The origin of the gourd-shaped etch pit should be a dislocation similar to the arrow-shaped etch pit.

Furthermore, Hanada *et al.*[43] pointed out that etch pits of various shapes were observed on (010) plane and divided into types A-G according to the shape of etch pits as shown in Figs. 12 and 13. The type-A etch pit became type-B etch pit after etching for 10 min, and subsequently became the type-C etch pit after further etching for 10 min. Finally, the type-C etch pit changed to type-D after etching for 20 more min. Therefore, it could be concluded that type A, B, C, and D originate from void-type crystal defects. The type-G void defect could become type-A etch pit after etching as shown in Fig. 13. Thus, the void defects must change in shape similar to type-G→A→B→C→D etch pits by etching. In addition, the size of the type-E and type-F etch pit increased after etching, nevertheless, the shape remained unchanged. This suggested that the type-E and type-F etch pit contained a dislocation as its core in the depth direction.
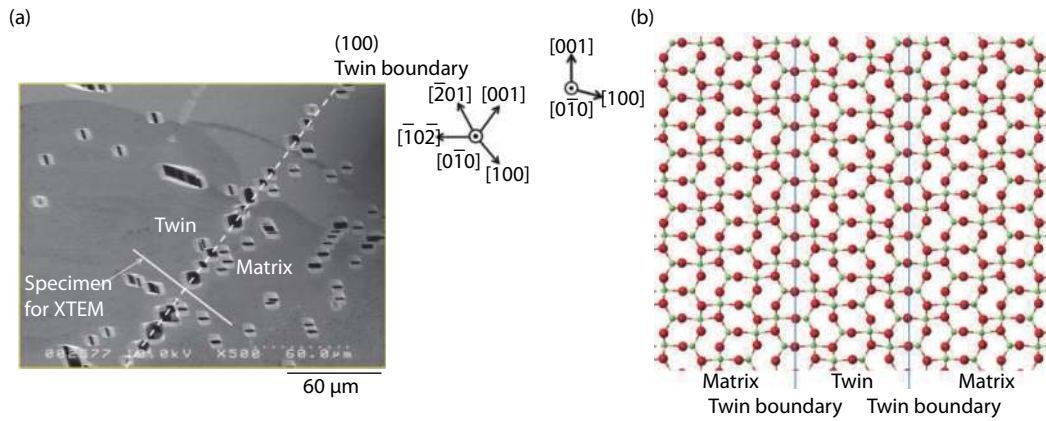
Fig. 9. (a) An SEM image of etched surface of $(0\bar{1}0)$ plane including a twin boundary. (b) The atomic structure of a region including a twin lamellae in β-Ga$_2$O$_3$ crystal viewed from the $(0\bar{1}0)$ direction. Copyright 2016 Jpn J Appl Phys[39].
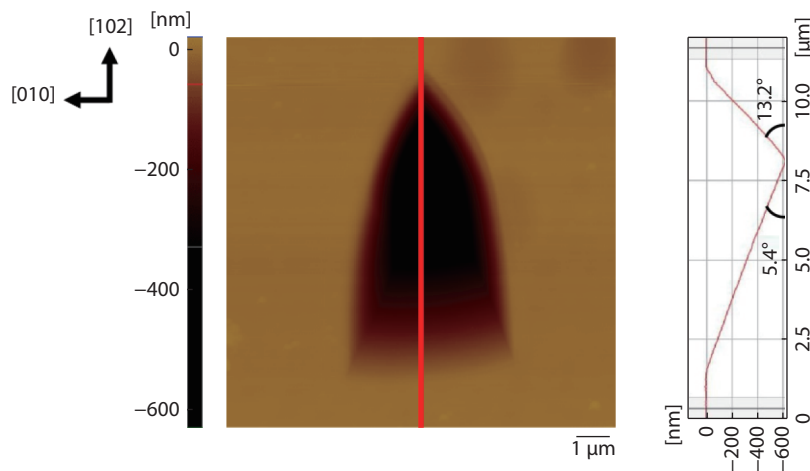

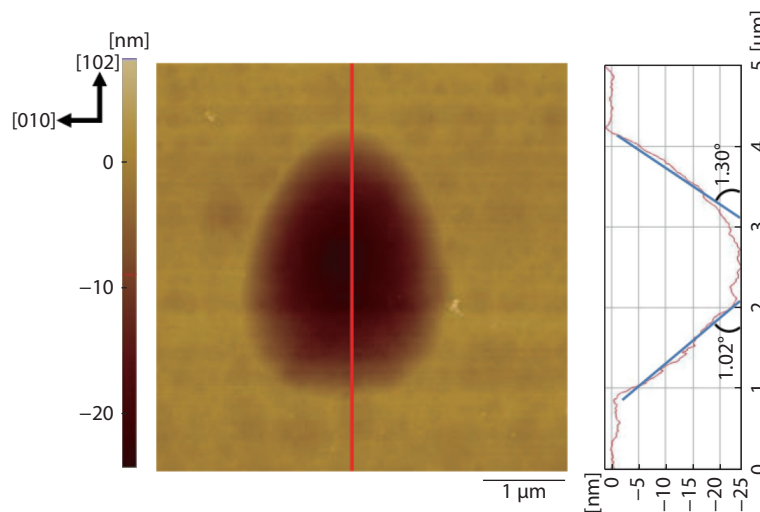Fig. 10. (Color online) AFM images of an arrow-shaped etch pit. Copyright 2017 Jpn J Appl Phys[45].

Fig. 11. (Color online) AFM image of a gourd-shaped etch pit. Copyright 2017 Jpn J Appl Phys[45].

2.5. Defects summary

Table 1 covers all types of defects, except small defects [discussed in 3.2], observed on different β-Ga$_2$O$_3$ crystal planes. Actually, in terms of defects features, these defects can be classified into three types: (1) dislocation (edge dislocation and screw dislocation)，(2) defects that originated from voids (hollow nanopipes, PNPs, NSGs, line-shaped grooves), (3) twin. The

Burgers vector of edge and screw dislocation observed on $(\bar{2}01)$ and (010) respectively are both paralleled to [010] direction. However, the distribution direction of etch pits and the dislocation extending direction are completely different. In addition, it is found that the extending direction of void defects are all paralleled to the [010] direction. The etch pits distribution of PNPs and NSGs observed on (010) lie in rows along [100]
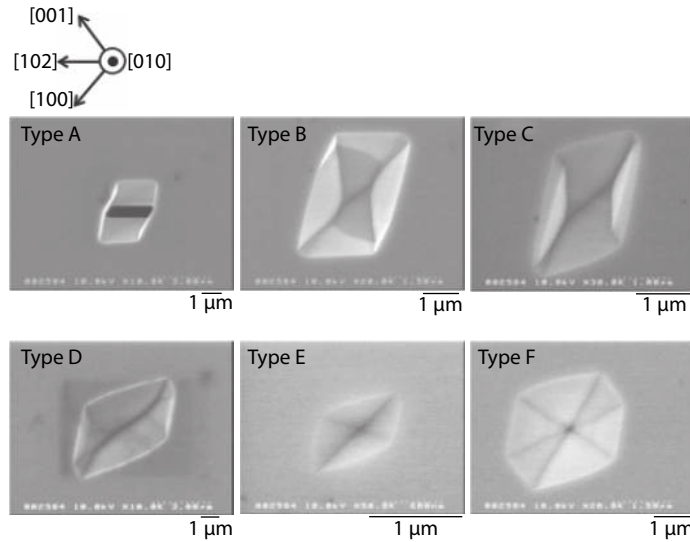
B Fu et al.: A review of β-Ga$_2$O$_3$ single crystal defects, their effects on device performance and ......

Fig. 12. SEM images of six etch pits of different shapes (Types A, B, C, D, E, and F) according to shapes of the etch pits on β-Ga$_2$O$_3$ (010) single crystal surface. Copyright 2016 Jpn J Appl Phys.[43]
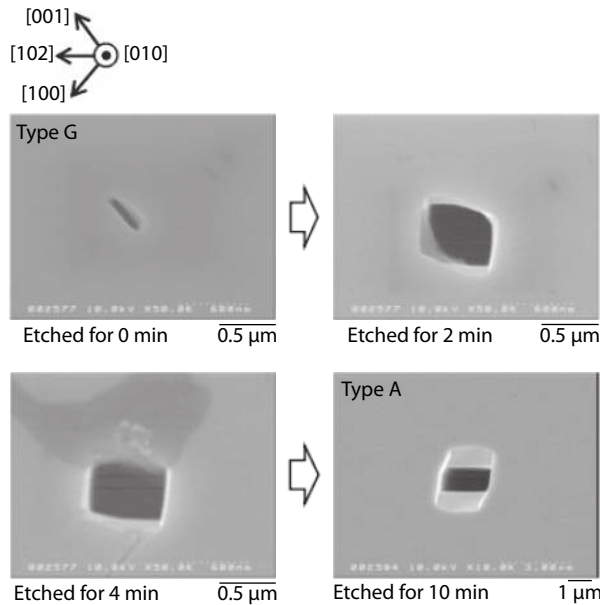

Fig. 13. SEM images of the same pit at the same position on the same β-Ga$_2$O$_3$ (010) single crystal surface etched for the etching times of 0, 2, 4, and 10 min. Copyright 2016 Jpn J Appl Phys[43].

Table 1.   All kinds of defects observed on different β-Ga$_2$O$_3$ crystal plane.

Parameter	Edge dislocation	Screw dislocation	Twin	Hollow nanopipes	PNPs	NSGs	Line-shaped grooves
Crystal plane	($\bar{2}$01)	(010)	(0$\bar{1}$0)	(010)	(010)	(010)	($\bar{2}$01)(001)
Crystal direction	//[010]	//[100]//[102]		No direction	//[100]	//[001]	No direction
Dislocation direction	Not exactly normal to ($\bar{2}$01) but slightly tilting to [102]	//[010]					
Burgers vector	//[010]	//[010]					
Twin plane			(100)				
Void direction				//[010]	//[010]	//[010]	//[010]

and [001] direction, respectively. Furthermore, the etch pits distribution of hollow nanopipes and line-shaped grooves observed on (010) and ($\bar{2}$01), (001) respectively do not show significant direction. The twin crystal found on (0$\bar{1}$0) is the (100) crystal plane.

3. Effects of the defects on device performance and their formation mechanism

3.1. Effects of the defects on device performance

In this section, four types of defects have been found in β-

B Fu et al.: A review of β-Ga$_2$O$_3$ single crystal defects, their effects on device performance and ......
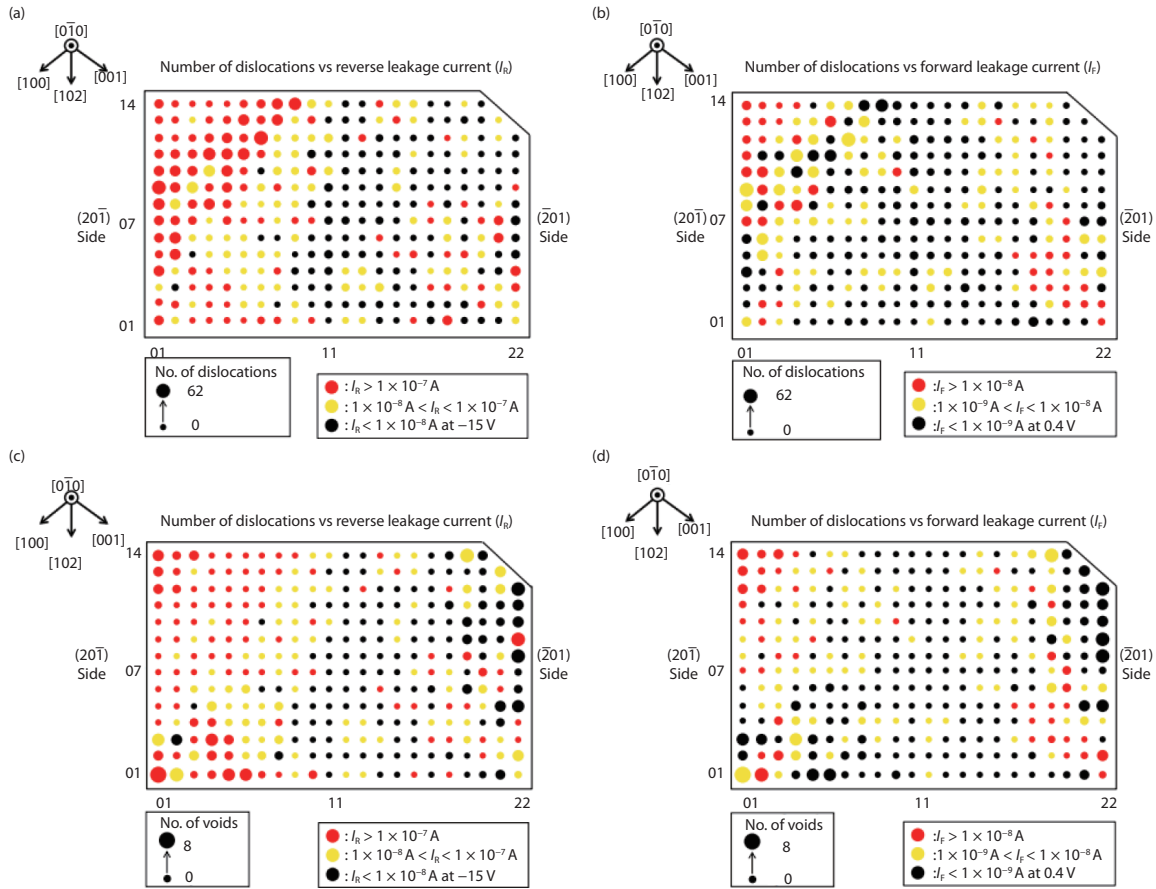
Fig. 14. (Color online) (a) Distributions of number of dislocations and reverse leakage current (I_R) in SBD. (b) Distributions of number of dislocations and forward leakage current (I_F) in SBDs. (c) Distributions of number of voids and reverse leakage current (I_R) in SBDs. (d) Distributions of number of voids and forward leakage current (I_F) in SBDs. Copyright 2016 Jpn J Appl Phys[48].

Ga$_2$O$_3$, and their effects on device performance are to be summarized. The effects on device performances caused by dislocation and void have been discussed by Kasu *et al*.[48] Fig. 14(a) showed the relationship between the number of dislocations and the reverse leakage current (I_R) in SBD. In this figure, the reverse leakage current at −15 V was represented by the colors of the circles. The black, yellow, and red circles indicated low, intermediate, and high reverse leakage currents (I_R), respectively. They found that in the rich dislocation region at the upper center to the middle right of the sample, the reverse leakage current (I_R) was high, which suggested that there was a strong relationship between the number of dislocations and the reverse leakage current. Dislocations were considered to run mainly along the [010] direction. Dislocation defects and their surroundings through the whole sample were regarded to act as a path of leakage current. Fig. 14(b) showed the relationship between the number of dislocations and the forward leakage current (I_F). In this figure, the forward leakage current was defined to be a current at a bias of 0.4 V. The forward leakage current (I_F) distribution seemed similar to the reverse leakage current (I_R) distribution.

Fig. 14(c) showed the relationship between the number of void etch pits and the reverse leakage current (I_R). The number of voids was represented by the diameter of the circle. The black, yellow, and red circles represented low, intermediate, and high reverse leakage currents (I_R), respectively. The SBDs in the lower left-hand region showed a large number of voids and a high leakage current. Therefore, the void defects in this re-

gion produced a leakage current.

In addition, on the right-hand side, SBDs with large number of dislocations showed a low reverse leakage current (black circles) in the Fig. 14(c). The void defects in this region, however, did not produce leakage current. Therefore, it seemed that not all void-type defects produce a leakage current. At present, it can be confirmed that voids were terminated within the crystal[40, 43]. Thus, some voids may become current paths between the (0$\bar{1}$0) surface and the (010) back face, but others may not. Fig. 14(d) showed the relationship between the number of voids and the forward leakage current. The forward leakage current showed a similar distribution to the reverse leakage current.

It is common knowledge that dislocation only terminates on crystal surface or boundary. In other words, once the dislocation is formed, it goes through the whole crystal plate easily. Subsequently, dislocation and the surrounding regions will act as paths for the leakage current of SBD in single crystal. However, not all voids produce leakage current. It not only depends on the orientation relationship between the extending direction of the void and the crystal plane, but also on the length of the void. The line-shaped grooves observed on the (001) and ($\bar{2}$01) did not alter the electrical properties because they rarely appeared on the surface and extended along [010] direction, which were paralleled to the substrate plane. On the other hand, some voids observed on (0$\bar{1}$0) caused the leakage current because they were long enough to run through the whole crystal plate and form a leakage current path from the
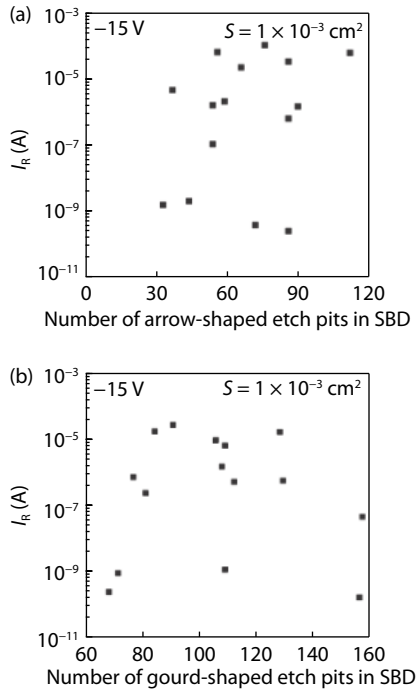
Fig. 15. (a) Relationship between the reverse leakage current and the number of arrow-shaped etch pits in SBD. (b) Relationship between the reverse leakage current and the number of gourd-shaped etch pits in SBD. The area of each SBD (S) is 1×10^{-3} cm^2. Copyright 2017 Jpn J Appl Phys[45].

$(0\bar{1}0)$ surface to the (010) back surface. That helped to understand why the etch pit density on the $(\bar{2}01)$ surface was higher than that on the (010) surface, but the number of SBDs with high leakage current on the $(\bar{2}01)$ surface was much lower than that on the (010) surface.

Apart from the defects of dislocation and void, it was not confirmed whether arrow-shaped etch pits[45] observed on the $(\bar{2}01)$ and (001) surface affected the electrical properties or not by using the etch-pitting method, as shown in Fig. 15(a). Similarly, there was no obvious relationship between the reverse leakage current and gourd-shaped etch pit density[45] on the $(\bar{2}01)$ surface as shown in Fig. 15(b). In addition, doping impurity was not related to the leakage current[44].

In addition to the reported effects of dislocation on the leakage current for power device above, the dislocation in β-Ga$_2$O$_3$ single crystal may have other impacts on the electrical properties. The dislocation may generate a large number of electrically active centers due to the uncoordinated atoms in the dislocation core, which can lead to the formation of new energy levels in the band gap. In addition, the dislocation may also change parameters related to carriers, such as carrier lifetime and mobility, because it can become the capture center of carriers[49, 50].

The effects of twin on electrical properties have not been reported up to now. However, the optical and electrical properties of β-Ga$_2$O$_3$ single crystal, such as photoabsorption and carrier characteristics, may change due to the existence of twin[51].

3.2. The formation mechanism of defects

It is of great importance to improve the quality of crystals by clarifying the formation mechanism of the defects, in order that they may provide adequate support for device performance. In Section 2.5, the defects observed in β-Ga$_2$O$_3$ crystal
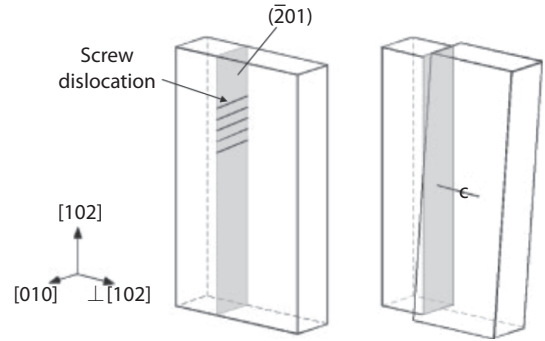

Fig. 16. Schematic of a subgrain boundary. Copyright 2015 Jpn J Appl Phys[38].

were divided into three types: dislocation, void and twin. However, the small defects, including the arrow-shaped and gourd-shaped etch pits, were not regarded as intrinsic defects. It is well known that the crystal plate must be polished before etching. Presently, chemical mechanic polishing (CMP) is very popular with wafer manufacture because it can cause little polishing scratch and mechanical damage compared with common mechanical polish. However, CMP also causes unintentional damage to wafers. Most small defects are induced by mechanical damages[44]. Therefore, they are not defined as the native defects in β-Ga$_2$O$_3$ single crystal.

The dislocation can be induced by many conditions when growing bulk single crystal. The common case is that the dislocations existing in crystals are caused by the extension of defect from the seed to the grown crystal. In most cases, that can be eliminated by the technology of "neck"[55, 56]. The dislocations can also be induced easily at the "seed" stage because of the thermal shock, which can be overcome and improved by extending the meltback distance of the seed[57]. In addition, crystalline interface morphology[58], stress[59], component segregation[60] and inclusion[61] can also lead to the occurence of dislocations. As for dislocations in β-Ga$_2$O$_3$ crystal, Nakai et al.[38] carried out a more detailed analysis. They interpreted that screw dislocations aligning along [102] form a subgrain boundary, as shown in Fig. 16. The subgrain boundary was a twist boundary with a rotation axis perpendicular to the boundary plane $(\bar{2}01)$. The rotation angle θ can be estimated from the following equation[53]:

$$\theta = b/D,$$

where b was the magnitude of the Burgers vector and D was the spacing between dislocations. So far, they have no TEM results of the dislocations under etch pits aligning along [100]. However, the shape of the etch pits was similar to that aligning along [102]. Therefore, they supposed that the defects under etch pits aligning along [100] were also screw dislocations.

Edge dislocations lying on a plane slightly tilted towards the (102) plane, with a possible slip plane being the (101) plane, which has also been reported by Yamaguchi et al.[52]. Since the generation mechanism of edge dislocations has not yet been proved, further researches are necessary to prove.

Indeed, both PNPs and NSGs can be classified as hollow nanopipes. These hollow nanopipes have no surrounding strain field, therefore, the formation mechanism of them are different from the defects of micropipe observed in SiC. The micropipe is known to be hollow with a diameter of 2–3 μm[37].

The formation mechanism is that a screw dislocation with a Burgers vector larger than a critical value of the order of 1.0 nm magnitude produces a hollow pipe in the core to reduce the strain energy around the dislocation[54]. Therefore, the micropipe has a large strain field that can be detected by X-ray topography. However, the nanopipe in β-Ga$_2$O$_3$ has no surrounding strain field, which suggests that the hollow nanopipe formation is not caused by a screw dislocation with a large Burgers vector. As is mentioned in Section 2.5 above, hollow nanopipes, PNPs, NSGs and line-shaped grooves were all originated from voids. Regarding the generation mechanisms for voids, Ueda *et al.* proposed the following conditions[39]:

(1) The condensation of excess oxygen vacancies in the grown crystal generates multiple vacancy-type stacking faults on the crystal plane and finally forms voids.

(2) The voids are formed by the penetration of tiny bubbles at the liquid–solid interface into grain boundaries.

(3) The voids are formed by local meltback at some grown-in defects such as screw-type dislocations during growth.

Up to now, numerous experiments and tests are being done in order to clarify the generation mechanism of voids, but no conclusion has been drawn.

Referring to the crystal growth methods related to CZ, twins are typical defects that often generate in the early stage, namely, the shoulder part of the bulk crystals. It is also well known that twins are assumed to be generated by strain relaxation during the crystal growth, and they can be suppressed by adjusting the growth conditions. Twins are originated commonly from the TPB point (intersection of liquid-solid-gas)[62]. Hurle summarized the three factors leading to the existence of twins easily when using CZ to grow crystal[63]:

(1) The facet at the position of TPB point appears on the crystal surface.

(2) Special shoulder angle is required to form the twin on the external surface and make the facet exist continuously. At the same time, the contact angle between the growing surface and the meniscus surface makes the tension balanced at the TPB point exactly.

(3) There is a big degree of supercooling outside the crystal surface.

As for the twins observed in β-Ga$_2$O$_3$ crystal[39], it was assumed that the nucleation of twin lamellae was an initial stage of the "shoulder part" during crystal growth. After the twin lamellae were nucleated, their width increased with the relaxation of accumulated strain in the grown crystal. However, the origin of the twin lamellae remains unclear at present. Further study needs to be conducted.

4. Conclusion

In this paper, we have presented four types of defects in β-Ga$_2$O$_3$ single crystal, discussed their effects on device performance and analyzed their formation mechanisms in detail.

Four types of defects, namely dislocations, voids, twin and small defects, were found in β-Ga$_2$O$_3$. The dislocations can be divided into two types, screw and edge dislocation. The hollow nanopipes, PNPs, NSGs and line-shaped grooves were originated from the voids defects. An important defect, twin, was observed on the (100) crystal plane.

The effects of those defects on device performance were also discussed. The dislocation and the surrounding regions can act as paths for the leakage current of SBD in single crystal. However, not all voids produced leakage current. It not only depended on the orientation relationship between the extending direction of the void and the crystal plane, but also on the length of the void. There's no strong evidence yet to show that the etch-pitting method plays a role in proving small defects affect the electrical properties. In addition, doping impurity was definitely not related to the leakage current.

The formation mechanism of defects in β-Ga$_2$O$_3$ single crystal was analyzed in detail. Most of the small defects, such as the arrow-shaped and gourd-shaped etch pits, were induced by mechanical damages. The screw dislocation was originated from a subgrain boundary. The edge dislocation lying on a plane slightly tilted towards the (102) plane, with the (101) plane being the possible slip plane. The voids defect, including hollow nanopipes, PNPs, NSGs and line-shaped grooves may be caused by the condensation of excess oxygen vacancies, the penetration of tiny bubbles or local meltback. The nucleation of twin lamellae was formed at an initial stage of the "shoulder part" during the crystal growth.

These findings also suggest that the formation of defects can be controlled by adjusting the growth condition of the bulk crystal and the subsequent substrate fabrication process. Thus, it is hopeful to fabricate devices with better electrical performance on β-Ga$_2$O$_3$ single crystal.

References

[1] Baldini M, Galazka Z, Wagner G. Recent progress in the growth of β-Ga$_2$O$_3$ for power electronics applications. Mater Sci Semicond Process, 2017, 78, 132

[2] Pearton S J, Yang J, Cary IV P H, et al. A review of Ga$_2$O$_3$ materials, processing, and devices. Appl Phys Rev, 2018, 5(1), 011301

[3] Jang S, Jung S, Beers K, et al. A comparative study of wet etching and contacts on (2⁻01) and (010) oriented β-Ga$_2$O$_3$. J Alloys Compd, 2018, 731, 118-125

[4] Ghose S. Growth and characterization of wide bandgap semiconductor oxide thin films. PhD Dissertations, Texas State University, 2017

[5] Stepanov S I, Nikolaev V I, Bougrov V E, et al. Gallium oxide: properties and applica a review. Rev Adv Mater Sci, 2016, 44, 63

[6] Harwig T, Wubs G J, Dirksen G J. Electrical properties of β-Ga$_2$O$_3$ single crystals. Solid State Commun, 1976, 18(9/10), 1223

[7] Chase A O. Growth of β-Ga$_2$O$_3$ by the Verneuil Technique. J Am Ceram Soc, 1964, 47(9), 470

[8] Lorenz M R, Woods J F, Gambino R J. Some electrical properties of the semiconductor β-Ga$_2$O$_3$. J Phys Chem Solids, 1967, 28(3), 403

[9] Víllora E G, Yamaga M, Inoue T, et al. Optical spectroscopy study on β-Ga$_2$O$_3$. Jpn J Appl Phys, 2002, 41(6A), L622

[10] Zhang J, Li B, Xia C, et al. Growth and spectral characterization of

β-Ga$_2$O$_3$ single crystals. J Phys Chem Solids, 2006, 67(12), 2448

[11] Víllora E G, Shimamura K, Yoshikawa Y, et al. Large-size β-Ga$_2$O$_3$ single crystals and wafers. J Cryst Growth, 2004, 270(3/4), 420

[12] Ohba E, Kobayashi T, Kado M, et al. Defect characterization of β-Ga$_2$O$_3$ single crystals grown by vertical Bridgman method. Jpn J Appl Phys, 2016, 55(12), 1202B

[13] Hoshikawa K, Ohba E, Kobayashi T, et al. Growth of β-Ga$_2$O$_3$ single crystals using vertical Bridgman method in ambient air. J Cryst Growth, 2016, 447, 36

[14] Hideo A, Kengo N, Hidetoshi T, et al. Growth of β-Ga$_2$O$_3$ single crystals by the edge-defined, film fed growth method. Jpn J Appl Phys, 2008, 47(11R), 8506

[15] Bell R O. Modeling of the time dependence of EFG crystal growth. J Cryst Growth, 1990, 104(1), 23

[16] Braescu L, Duffar T. Effect of buoyancy and Marangoni forces on the dopant distribution in a single crystal fiber grown from the melt by edge-defined film-fed growth (EFG) method. J Cryst Growth, 2008, 310(2), 484

[17] Bunoiu O, Nicoara I, Santailler J L, et al. Fluid flow and solute segregation in EFG crystal growth process. J Cryst Growth, 2005, 275(1/2), e799

[18] Galazka Z, Uecker R, Fornari R. A novel crystal growth technique from the melt: levitation-assisted self-seeding crystal growth method. J Cryst Growth, 2014, 388, 61

[19] Shimamura K, Villora E G. Czochralski-Based growth and characteristics of selected novel single crystals for optical applications. Acta Phys Polon A, 2013, 124(2), 265

[20] Galazka Z, Uecker R, Irmscher K, et al. Czochralski growth and characterization of β-Ga$_2$O$_3$ single crystals. Cryst Res Technol, 2010, 45(12), 1229

[21] Irmscher K, Galazka Z, Pietsch M, et al. Electrical properties of β-Ga$_2$O$_3$ single crystals grown by the Czochralski method. J Appl Phys, 2011, 110(6), 063720

[22] Tomm Y, Reiche P, Klimm D, et al. Czochralski grown Ga$_2$O$_3$ crystals. Jpn J Appl Phys, 2000, 220(4), 510

[23] Galazka Z, Uecker R, Klimm D, et al. Scaling-up of bulk β-Ga$_2$O$_3$ single crystals by the Czochralski method. ECS J Solid State Sci Technol, 2017, 6(2), Q3007

[24] Katz G, Roy R. Flux Growth and characterization of β-Ga$_2$O$_3$ single crystals. J Am Ceram Soc, 1966, 49(3), 168

[25] Chani V I, Inoue K, Shimamura K, et al. Segregation coefficients in β-Ga$_2$O$_3$:Cr crystals grown from a B$_2$O$_3$ based flux. J Cryst Growth, 1993, 132(1/2), 335

[26] Matsumoto T, Aoki M, Kinoshita A, et al. Absorption and reflection of vapor grown single crystal platelets of β-Ga$_2$O$_3$. Jpn J Appl Phys, 1974, 13, 1578

[27] Juskowiak H, Pajaczkowska A. Chemical transport of β-Ga$_2$O$_3$ using chlorine as a transporting agent. J Mater Sci, 1986, 21(10), 3430

[28] Mastro M A, Kuramata A, Calkins J, et al. Perspective—opportunities and future directions for Ga$_2$O$_3$. ECS J Solid State Sci Technol, 2017, 6(5), 356

[29] Higashiwaki M, Sasaki K, Kuramata A, et al. Development of gallium oxide power devices. Physl Status Solidi A, 2014, 211(1), 21

[30] Shimamura K, Víllora E G, Domen K, et al. Epitaxial growth of GaN on (1 0 0) β-Ga$_2$O$_3$ substrates by metalorganic vapor phase epitaxy. Jpn J Appl Phys, 2004, 44(1L), L7

[31] Wellmann P J. Power electronic semiconductor materials for automotive and energy saving applications–SiC, GaN, Ga$_2$O$_3$, and diamond. Zeitschrift für anorganische und allgemeine Chemie, 2017, 643(21), 1312

[32] Higashiwaki M, Sasaki K, Kuramata A, et al. Gallium oxide (Ga$_2$O$_3$) metal–semiconductor field-effect transistors on single-crystal β-Ga$_2$O$_3$ (010) substrates. Appl Phys Lett, 2012, 100(1), 013504

[33] Higashiwaki M, Sasaki K, Murakami H, et al. Recent progress in Ga$_2$O$_3$ power devices. Semicond Sci Technol, 2016, 31(3), 034001

[34] Ma N, Tanen N, Verma A, et al. Intrinsic electron mobility limits in β-Ga$_2$O$_3$. Appl Phys Lett, 2016, 109(21), 212101

[35] Fujita S. Wide-bandgap semiconductor materials: For their full bloom. Jpn J Appl Phys, 2015, 54(3), 030101

[36] Burns R P. Systematics of the evaporation coefficient Al$_2$O$_3$, Ga$_2$O$_3$, In$_2$O$_3$. J Chem Phys, 1966, 44(9), 3307

[37] Takahashi J, Kanaya M, Fujiwara Y. Sublimation growth of SiC single crystalline ingots on faces perpendicular to the (0001) basal plane. J Cryst Growth, 1994, 135(1/2), 61

[38] Nakai K, Nagai T, Noami K, et al. Characterization of defects in β-Ga$_2$O$_3$ single crystals. Jpn J Appl Phys, 2015, 54(5), 051103

[39] Ueda O, Ikenaga N, Koshi K, et al. Structural evaluation of defects in β-Ga$_2$O$_3$ single crystals grown by edge-defined film-fed growth process. Jpn J Appl Phys, 2016, 55(12), 1202B

[40] Hanada K, Moribayashi T, Uematsu T, et al. Observation of nanometer-sized crystalline grooves in as-grown β-Ga$_2$O$_3$ single crystals. Jpn J Appl Phys, 2016, 55(3), 030303

[41] Neudeck P G, Powell J A. Performance limiting micropipe defects in silicon carbide wafers. IEEE Electron Device Lett, 1994, 15(2), 63

[42] Crimp M A, Simkin B A, Ng B C. Demonstration of the g· bxu = 0 edge dislocation invisibility criterion for electron channelling contrast imaging. Philosophical Magazine Letters, 2001, 81(12), 833

[43] Hanada K, Moribayashi T, Koshi K, et al. Origins of etch pits in β-Ga$_2$O$_3$ (010) single crystals. Jpn J Appl Phys, 2016, 55(12), 1202B

[44] Oshima T, Hashiguchi A, Moribayashi T, et al. Electrical properties of Schottky barrier diodes fabricated on (001) β-Ga$_2$O$_3$ substrates with crystal defects. Jpn J Appl Phys, 2017, 56(8), 086501

[45] Kasu M, Oshima T, Hanada K, et al. Crystal defects observed by the etch-pit method and their effects on Schottky-barrier-diode characteristics on (-201) β-Ga$_2$O$_3$. Jpn J Appl Phys, 2017, 56(9), 091101

[46] Kuramata A, Koshi K, Watanabe S, et al. High-quality β-Ga$_2$O$_3$ single crystals grown by edge-defined film-fed growth. Jpn J Appl Phys, 2016, 55(12), 12022

[47] Galazka Z, Irmscher K, Uecker R, et al. On the bulk β-Ga$_2$O$_3$ single crystals grown by the Czochralski method. J Cryst Growth, 2014, 404, 184

[48] Kasu M, Hanada K, Moribayashi T, et al. Relationship between crystal defects and leakage current in β-Ga$_2$O$_3$ Schottky barrier diodes. Jpn J Appl Phys, 2016, 55(12), 1202B

[49] Assali L V C. Electrically active centers in partial dislocations in semiconductors. Physica B, 2001, 308, 489

[50] Capan I, Borjanović V, Pivac B. Dislocation-related deep levels in carbon rich p-type polycrystalline silicon. Sol Energy Mater Sol Cells, 2007, 91(10), 931

[51] Ikonić Z, Srivastava G P, Inkson J C. Electronic properties of twin boundaries and twinning superlattices in diamond-type and zinc-blende-type semiconductors. Phys Rev B, 1993, 48(23), 17181

[52] Yamaguchi H, Kuramata A, Masui T. Slip system analysis and X-ray topographic study on β-Ga$_2$O$_3$. Superlattices Microstruct, 2016, 99, 99

[53] Read W T. Dislocations in crystals. New York: McGraw-Hill, 1953.

[54] Frank F C. Capillary equilibria of dislocated crystals. Acta Crystallographica, 1951, 4(6), 497

[55] Dash W C. Silicon crystals free of dislocations. J Appl Phys, 1958, 29(4), 736

[56] Dash W C. Improvements on the pedestal method of growing silicon and germanium crystals. J Appl Phys, 1960, 31(4), 736

[57] Taishi T, Huang X, Yonenaga I, et al. Behavior of the edge dislocation propagating along the growth direction in Czochralski Si crystal growth. J Cryst Growth, 2005, 275(1/2), e2147

[58] Taishi T, Ohno Y, Yonenaga I, et al. Influence of seed/crystal interface shape on dislocation generation in Czochralski Si crystal

growth. Physica B, 2007, 401, 560

[59] Noor J W, Dam B. The growth spiral morphology on {100} KDP related to impurity effects and step kinetics. J Cryst Growth, 1986, 76(2), 243

[60] Tiller W A. The science of crystallization: macroscopic phenomena and defect generation. Cambridge University Press, 1991

[61] Chaldyshev V V, Kolesnikova A L, Bert N A, et al. Investigation of dislocation loops associated with As–Sb nanoclusters in GaAs. J Appl Phys, 2005, 97(2), 024309

[62] Neubert M, Kwasniewski A, Fornari R. Analysis of twin formation in sphalerite-type compound semiconductors: A model study on bulk InP using statistical methods. J Cryst Growth, 2008, 310(24), 5270

[63] Chung H, Dudley M, Larson D J Jr, et al. The mechanism of growth-twin formation in zincblende crystals: new insights from a study of magnetic liquid encapsulated Czochralski-grown InP single crystals. J Cryst Growth, 1998, 187(1), 9